

in X-ray novae. Beyond this, there are properties that, taken together, are usually considered to be indicative of black-hole systems¹⁴. They are: (1) an ultra-soft spectrum in the 1–10 keV band, (2) a hard spectral component which extends to several hundred keV, and (3) broad-band, short timescale variability ($1-10^{-3}$ s), usually when the hard spectral component is present. The TTM–Kvant–Mir team reported an ultra-soft spectrum for GRO J1655–40 on 24 and 25 September with a black-body temperature¹⁶ of 1 keV. Rosat observations¹⁷ show flux variability on timescales down to 0.1 s in the 0.1–1 keV energy band. Although more detailed studies of possible short-timescale variability of the source are underway (D. Cray *et al.*, manuscript in preparation), the standard all-sky monitoring routines performed daily on BATSE background data showed no prominent variability or pulsed emission from the direction of GRO J1655–40 in the time range of 3–300 s at 10% of the peak flux level observed in Fig. 1. The current observational constraints therefore favour the presence of a black hole in GRO J1655–40.

Theoretical arguments indicate that jet-like or collimated supersonic flows can arise from radiation-pressure dominated disks, where mass flow to the inner disk can feed loosely collimated jets of material¹.

A consistent relationship between the hard X-ray and radio fluxes and the plasma ejection times is observed in three distinct episodes of GRO J1655–40. This supports the interpretation that feeding of material into jets occurs in the inner disk, as that is also the most likely site of hard X-ray production. The varying delay times between the X-ray and radio secondary peaks, and the general tendency away from a simple one-to-one relationship between fluxes in the two wavelength bands, indicate that the ejection mechanism is not strictly determined by a critical luminosity as determined from the hard X-ray flux alone. We note that intense soft X-ray fluxes have been detected¹⁶ when the hard X-ray flux as determined by BATSE was relatively weak. Further, we find that the hard X-ray flux shows significant variability on a timescale of hours, and a degree of anti-correlated behaviour with the radio flux, usually after the X-ray flux has reached a maximum. This would suggest that the emission of X-rays and γ -rays is being suppressed by a change of state in the inner disk rather than simply decreasing in response to a reduction in accretion rate.

It is interesting to compare this source with the transient source GRS 1915+105. This object was discovered in August 1992 with GRANAT/WATCH¹⁸ and reported recently by Mirabel and Rodriguez¹⁹ to be a radio source with superluminal jets. Although GRS 1915+105 has a hard X-ray spectrum²⁰ similar to GRO J1655–40, it has not been considered an X-ray nova due to its long risetime²¹. It has undergone long-duration flares since 1992 in hard X-rays²¹ and radio flares up to 1 Jy from 1992 to 1994¹⁹. It is variable over hours to days, and episodes of strong X-ray emission lasting several weeks are interspersed with quiescent periods (K. Deal *et al.*, manuscript in preparation). The dramatic variability of the hard X-rays seen in these two transients would appear to be related to the presence of the radio jets; however, more detailed correlative studies will have to be done. □

Received 21 October 1994; accepted 10 March 1995.

1. Begelman, M. C., Blandford, R. D. & Rees, M. J. *Rev. mod. Phys.* **56**, 255–351 (1984).
2. Zhang, S. N. *et al.* *IAU Circ.* No. 6046 (1994).
3. Wilson, C. A. *et al.* *IAU Circ.* No. 6056 (1994).
4. Fishman, G. J. *et al.* in *Gamma Ray Observatory Science Workshop* (eds Shrader, C. R., Gehrels, N. & Dennis, B.) 2-39–2-50 (CP-3137, NASA, Greenbelt, Maryland, USA, 1989).
5. Zhang, S. N., Fishman, G. J., Harmon, B. A. & Paciesas, W. S. *Nature* **366**, 245–247 (1993).
6. Baijyn, C. D. *et al.* *Nature* **374**, 701–703 (1995).
7. Campbell-Wilson, D. & Hunstead, R. *IAU Circ.* Nos 6052 & 6055 (1994).
8. Campbell-Wilson, D., McKay, D. J. & Lovell, J. E. *IAU Circ.* No. 6078 (1994).
9. Hjellming, R. M. & Rupen, M. P. *Nature* (submitted).
10. Press, W. H. *et al.* *Numerical Recipes in Fortran 2nd edn* 569–577 (Cambridge Univ. Press, 1992).
11. Kroeger, R. A., Grove, J. E., Kurfess, J. D., Johnson, W. N. & Strickman, M. S. *IAU Circ.* No. 6051 (1994).
12. McKay, D. & Kesteven, M. *IAU Circ.* No. 6062 (1994).
13. Tingay, S. J. *et al.* *Nature* **374**, 141–143 (1995).

14. White, N. E. in *The Evolution of X-ray Binaries* (eds Holt, S. S. & Day, C. S.) 53–60 (AIP Conf. Proc. 308, Am. Inst. Physics, New York, 1994).
15. Van Paradijs, J. & McClintock, J. in *X-Ray Binaries* (eds Lewin, W. H. G. & v. d. Heuvel, E. P. J.) (Cambridge Univ. Press, in the press).
16. Alexandrovich, N., Borozdin, K., Efremov, V. & Sunyaev, R. *IAU Circ.* No. 6087 (1994).
17. Greiner, J. *IAU Circ.* No. 6078 (1994).
18. Sazonov, S. Yu. *et al.* *Astr. Lett.* **20**, 787–791 (1994).
19. Mirabel, I. F. & Rodriguez, L. F. *Nature* **371**, 46–48 (1994).
20. Finoguenov, A. *et al.* *Astrophys. J.* **424**, 940–942 (1994).
21. Harmon, B. A. *et al.* in *The Second Compton Symposium* (eds Fichtel, C. E., Gehrels, N. & Norris, J. P.) 210–219 (AIP Conf. Proc. 304, Am. Inst. Physics, New York, 1993).

ACKNOWLEDGEMENTS. We thank J. van Paradijs for useful comments. The National Radio Astronomy Observatory is operated by Associated Universities Incorporated under a cooperative agreement with the US NSF.

Waves from the collisions of comet Shoemaker–Levy 9 with Jupiter

Andrew P. Ingersoll & Hiroo Kanamori

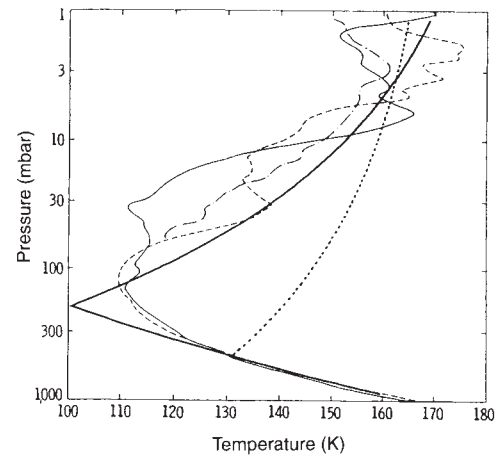
Division of Geological and Planetary Sciences,
California Institute of Technology, Pasadena,
California 91125, USA

OBSERVATIONS of the collisions of the fragments of comet Shoemaker–Levy 9 with Jupiter provided an unprecedented opportunity to probe the depths of the planet's atmosphere. Images taken by the Hubble Space Telescope revealed circular rings surrounding five of the impact sites¹. The rings were observed for up to 2.5 hours after the impacts and spread at a constant velocity of 450 m s^{-1} . There are three types of disturbance that might explain these observations: acoustic waves trapped at the tropopause temperature minimum², gravity waves propagating vertically and horizontally in the stratosphere³, and gravity waves trapped in a stable layer which acts as a horizontal waveguide and is located within the hypothesized tropospheric water cloud⁴. Here we show that only the last of these phenomena can match the speed and relative amplitude of the observed waves, with the requirement that the impacts were deep and the stability of the trapping layer is large. The origin of the stable layer is still uncertain, but if it is produced by moist convection in the water cloud, then the ratio of oxygen to hydrogen on Jupiter must be surprisingly large—approximately ten times that on the Sun.

Rings were seen after impacts A, E, G, Q1 and R. In a plot of ring radius r versus time t , the points from the different impacts all lie on the same straight line. The slope gives the speed, which is 450 m s^{-1} . The intercept gives the initial radius, $r = 500 \text{ km}$ at $t = 0$. Impact sites E and G also have a faint inner ring, the speed of which is uncertain but is in the range $180-350 \text{ m s}^{-1}$. The ring material seems to be impact debris. Images taken through a methane filter, in which high-altitude clouds appear bright, suggest that the ring material is located in the stratosphere somewhere between the 1- and 300-mbar levels^{1,5}.

The observed constant velocity suggests that the rings are propagating waves. The velocity would decrease with time if the particles were carried (advected) with the disturbance. This is because advection is a nonlinear process—the speed of propagation depends on the amplitude. Because the amplitude decays with time due to geometrical spreading, the speed should decrease with time if advection occurred. West *et al.*⁵ argue convincingly that the particles are created by condensation and destroyed by evaporation as the wave moves past. Other evidence of wave-like behaviour is that the points from different impacts fall on the same straight line in the plot of radius versus time. If material were flowing outwards behind a shock wave or other nonlinear disturbance, the speed would depend on the

FIG. 1 Temperature profiles as measured by Voyager (dashed, dot-dashed, and light solid lines)⁷ and as used in the gravity-wave model (dotted and heavy solid lines). The wiggles in the measured profiles are real, making it difficult to define the 'true' profile. The model profile⁴ on the right (dotted line) gives the right amount of leakage of wave energy into the stratosphere⁹. The profile on the left (heavy solid line) provides a better fit to the temperatures in terms of least-squares error. Our conclusions are the same regardless of which profile is used.



energy of impact, and the points would fall on different lines. For a linear wave, the speed depends only on properties of the medium. Nonlinear effects near the source could account for the finite initial radius of the ring.

We have calculated the amplitudes and speeds of sound waves and gravity waves for an impact energy of 10^{27} erg. We use linear theory, so amplitude scales with the energy. By "amplitude" we mean the lagrangian temperature perturbation at the 50-mbar level, near where the impact debris resides. Sound-wave amplitudes must be small, because no waves were seen travelling at the speed of sound. Even at the tropopause, where the temperature has its minimum value of 110 K, the speed of sound is 770 m s^{-1} , which is too fast to match the observations.

Following Kanamori², we represent sound waves from the impacts as a superposition of vertical normal modes. The fundamental ($n=0$) mode is incompressible, and has no temperature perturbation⁶. The $n=1$ mode represents energy trapped in the horizontal waveguide located at the temperature minimum near the 100-mbar level (that is, where $P=100$ mbar). The temperature profile is a digitized representation of the Voyager data⁷ shown in Fig. 1. The largest amplitude is associated with the trapped mode, and is $\pm 35 \text{ K}$ for a source near the temperature minimum (Fig. 2). For deeper sources the response is smaller, for example, $\pm 0.65 \text{ K}$ and $\pm 0.20 \text{ K}$ for sources at the 5- and 10-bar levels, respectively. As sound waves were not seen, the energy release must have been deep. A deep source is not inconsistent with the appearance of the fireball⁸ at later times and higher altitudes.

Following Ingersoll *et al.*⁴, we study gravity waves for a hydrostatic fluid on a rotating plane—an f -plane, in which the interaction of rotation and spherical geometry is neglected. Vertical structure follows Voyager data⁷ in the stratosphere and a moist

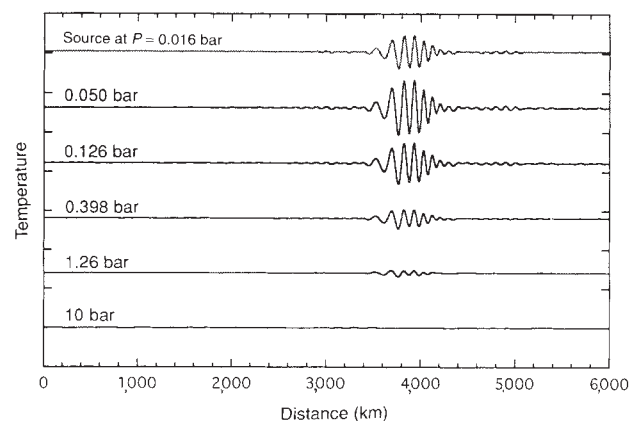
adiabat in the troposphere⁹, both fitted to simple analytical functions (Fig. 1, and Fig. 1 of ref. 4). The top of the model is an isothermal stratosphere extending to infinity at temperature $T_\infty = 185 \text{ K}$. The response to an impact includes both stratospheric gravity waves (SGWs), which propagate vertically, and tropospheric gravity waves (TGWs) which are trapped in the water cloud. The latter has a stable (sub-adiabatic) structure that is maintained by latent heat release and therefore depends on the jovian water abundance.

We define $e_{\text{H}_2\text{O}}$ as the enhancement factor of water relative to the solar abundance, that is, the jovian O/H ratio relative to that on the Sun. The speed of the TGW varies⁴ as $e_{\text{H}_2\text{O}}^{1/2}$, and for $e_{\text{H}_2\text{O}}=1$ the speed is 130 m s^{-1} . So if the rings were associated with TGWs, the observed speed of 450 m s^{-1} would imply $e_{\text{H}_2\text{O}} \approx 10$.

Figure 3 shows three of the heating profiles used in our calculations⁴. The abscissa is J , the energy deposited per unit pressure interval, and is related to energy/mass. All three profiles have $\int J dP = 10^{27}$ erg. (We use $\alpha^{-1} = P_m$, which is defined following equation (3) of ref. 4.) The cloud base is deep, near the 20-bar level, because we have assumed $e_{\text{H}_2\text{O}} \approx 10$. The $\alpha=0$ profile has energy deposited near the cloud base, the $\alpha=1$ profile is an intermediate case, and the $\alpha=5$ profile has energy deposited mostly in the stratosphere. In all cases heating is zero below cloud base.

Figure 4 shows our calculation of gravity waves 2 h (7,200 s) after the impact, using the temperature profile shown as a heavy solid line in Fig. 1 with $e_{\text{H}_2\text{O}} \approx 10$. The abscissa is radial distance r from the impact point. The ordinate is the lagrangian temperature perturbation at the 45-mbar level. The pulse at $r = 3,300 \text{ km}$ is the stratospheric 'tail' of the TGW travelling at 450 m s^{-1} . As in Fig. 2 of ref. 4, the disturbance amplitude is considerably

FIG. 2 Temperature perturbation versus distance for the acoustic-wave model, 5,400 s (1.5 h) after the impact; the energy of impact is 10^{27} erg. The curves show the temperature change experienced by a parcel at the 126-mbar level, for six different altitudes of energy input (all the energy goes in at one level); on the vertical axis, one division represents 50 K. The response drops as the depth increases. For a source at 5 bar the amplitude is $\pm 0.65 \text{ K}$; for a source at 10 bar the amplitude is $\pm 0.20 \text{ K}$. The speed of the wave packets is 725 m s^{-1} , which is faster than that seen in the Hubble Space Telescope images.



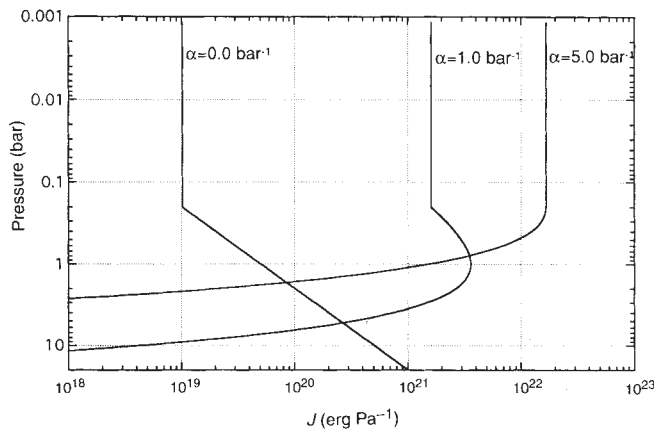


FIG. 3 Heating profiles for the gravity-wave model, defined following equation (3) of ref. 4, with $\alpha = 1/P_m$. Heating is expressed in terms of J , the energy deposited per unit pressure interval, with $\int J dP = 10^{27}$ erg. The model has 10 times the solar abundance of oxygen. The base of the water cloud is at 20 bar, and $J = 0$ below this level.

larger at 45 mbar than it is at 1 bar or at the ammonia cloud tops near 500 mbar.

The disturbance at $r = 6,700$ km is the leading edge of the SGW. Its speed is 930 m s^{-1} . We have run simulations where $e_{\text{H}_2\text{O}}$ has ranged from 0.5 to 10; we have tried putting all the heat at one level, varying the pressure of the level from 10 mbar to 10 bar; we have increased the pressure at the tropopause by a factor of three (Fig. 1, dotted line); and we have varied T_∞ . We find that the speed of the TGW depends only on $e_{\text{H}_2\text{O}}$. The speed of the SGW depends only on T_∞ , varying as $T_\infty^{1/2}$, and does not match the 450 m s^{-1} observed speed for any reasonable profile. Also in all our simulations, the amplitude of the SGW is less than that of the TGW. We conclude that the observed waves are TGWs, not SGWs.

The numerical model of Harrington *et al.*³ has five vertical layers. The top layer, with its base at 16 mbar, is a 'sponge' whose dynamics are dominated by Rayleigh friction. In contrast to our results, Harrington *et al.*³ found SGWs with speeds of 400 m s^{-1} . We can reproduce their result by replacing our semi-infinite stratosphere with a free surface (pressure perturbation = 0) at 16 mbar. The free surface reflects upward-propagating

waves; a sponge does the same, in models with low vertical resolution¹⁰. Reflection creates a stratospheric waveguide that changes the wave speeds. But in the real atmosphere, fast waves like these are not reflected.

In our model there is a second wave that travels at one-third the speed of the first (Fig. 4). These are⁴ the second and first modes of the tropospheric waveguide, spanning three quarter-cycles and one quarter-cycle, respectively, from cloud base to tropopause. The two modes might be related to the inner and outer rings, although the ratio of the two speeds (1:3 in the model) does not exactly match the observed ratio ($\sim 1:2$). This could be a failure to match the shape of the tropospheric temperature profile. The problem goes beyond our use of simple analytical functions, as the true profile is unlikely to follow a moist adiabat exactly.

Other inferences about the abundance of jovian water tend to support $e_{\text{H}_2\text{O}} \geq 1$, but there are major uncertainties. Bjoraker *et al.* observed water spectroscopically and inferred $e_{\text{H}_2\text{O}} \approx 1/50$. Analysing the same data, Carlson *et al.*¹² conclude that $e_{\text{H}_2\text{O}} \geq 1$, and argue that $e_{\text{H}_2\text{O}} = 10$ fits the data equally well (see Fig. 9 in ref. 12). Voyager and Earth-based observations¹³ give $e_{\text{CH}_4} \approx e_{\text{NH}_3} \approx 2$ and $e_{\text{He}} \approx 0.7$. Analysis of the gravitational harmonics of Jupiter¹⁴ suggests at least a five-fold enhancement of relatively heavy elements like oxygen, carbon and nitrogen. This predicted enhancement drops by a factor of two if Jupiter has a sub-adiabatic (radiative) zone in the 1–40 kbar pressure range, as suggested by Guillot *et al.*¹⁵.

Our work will be tested when the Galileo spacecraft encounters Jupiter in December 1995. We predict that it will find a deep stable layer extending down to the 20-bar level. Our best guess is that this layer is maintained by moist convection, with $e_{\text{H}_2\text{O}} \approx 10$. Such a result has important implications for our understanding of the origin of Jupiter, its internal history, and the chemistry and meteorology of its current atmosphere. □

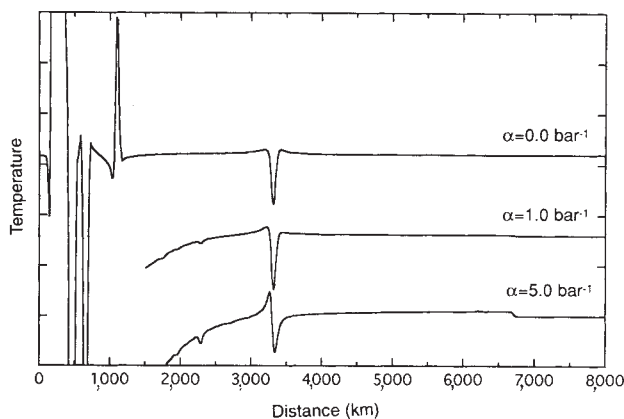


FIG. 4 Temperature perturbation at the 45-mbar level for the gravity-wave model, 7,200 s (2 h) after the impact; the energy of impact is 10^{27} erg. The unit is 1 K per division on the vertical axis. The abscissa is radial distance r from the impact point. The pulse at $r = 3,300$ km is the tropospheric gravity wave (TGW) that propagates in the water cloud. The water abundance ($e_{\text{H}_2\text{O}} \approx 10$) was chosen so that the speed of the TGW matches the 450 m s^{-1} observed speed. The pulse at $r = 1,100$ km is the second mode of the TGW. Its amplitude is off-scale for the lower two curves. The disturbance at $r = 6,700$ km is the stratospheric gravity wave (SGW). Its amplitude increases with α as the altitude of energy deposition rises (Fig. 3), but is always less than that of the TGW. The speed of the SGW is 930 m s^{-1} , which is more than twice the observed speed.

Received 24 February; accepted 22 March 1995.

- Hammel, H. B. *et al.* *Science* **267**, 1288–1296 (1995).
- Kanamori, H. *Geophys. Res. Lett.* **20**, 2921–2924 (1993).
- Harrington, J., LeBeau, R. P., Backes, K. A. & Dowling, T. E. *Nature* **368**, 525–527 (1994).
- Ingersoll, A. P., Kanamori, H. & Dowling, T. E. *Geophys. Res. Lett.* **21**, 1083–1086 (1994).
- West, R. A. *et al.* *Science* **267**, 1296–1301 (1995).
- Goldreich, P. & Kumar, P. *Astrophys. J.* **363**, 694–704 (1990).
- Lindal, G. F. *et al.* *J. Geophys. Res.* **86**, 8721–8727 (1981).
- Carlson, R. W. *et al.* *Geophys. Res. Lett.* (in the press).
- Achterberg, R. K. & Ingersoll, A. P. *J. Atmos. Sci.* **46**, 2448–2462 (1989).
- Lindzen, R. S., Batten, E. S. & Kim, J. W. *Mon. Weath. Rev.* **96**, 133–140 (1968).
- Bjoraker, G. L., Larson, H. P. & Kunde, V. G. *Icarus* **66**, 579–609 (1986).
- Carlson, B. E., Lacy, A. A. & Rossow, W. B. *Astrophys. J.* **388**, 648–668 (1992).
- Gautier, D. & Owen, T. in *Origin and Evolution of Planetary and Satellite Atmospheres* (eds Atreya, S. K., Pollack, J. B. & Matthews, M. S.) 487–512 (Univ. Arizona Press, Tucson, 1989).
- Hubbard, W. B. in *Origin and Evolution of Planetary and Satellite Atmospheres* (eds Atreya, S. K., Pollack, J. B. & Matthews, M. S.) 539–563 (Univ. Arizona Press, Tucson, 1989).
- Guillot, T., Chabrier, G., Morel, P. & Gautier, D. *Icarus* **112**, 354–357 (1994).

ACKNOWLEDGEMENTS. A.P.I. was supported by NASA's Planetary Atmospheres Program and NASA's Space Telescope Science Institute; H.K. was supported by the US NSF.